nature geoscience

Supplementary information

https://doi.org/10.1038/s41561-024-01564-5

Sustained greening of the Antarctic Peninsula observed from satellites

In the format provided by the authors and unedited

Supplementary Information: Sustained greening of the Antarctic Peninsula observed from satellites

Supplement 1. Data:

1.1 Imagery date selection

Satellite revisit times over the AP are comparable to other areas of the world, but cloud cover in coastal Antarctica is on average per year around 80-90%[1], which severely restricts the availability of suitable imagery. Our initial analysis demonstrated that data was most abundant in March, at the end of the austral summer and therefore coinciding with reduced snow cover (Supplementary Table 1.1).

Supplementary Table 1.1. Differences across January, February and March Landsat image NDVI > 0.2 and masked pixel area measurements for hexagons where moss banks have been observed in the field. “Best” values for the purpose of the study are shaded green i.e. high image availability, high measured vegetated area, and low pixel masking. Images taken in March measure the maximum extent and larger areas of vegetation on average.

	January	February	March
Image Count	270	289	233
Mean NDVI >0.2 Area (inc. Area = 0) (m^2)	1.03E+05	7.15E+04	1.34E+05
Standard Deviation	4.56E+05	3.26E+05	6.28E+05
Mean NDVI >0.2 Area (Area >0) (m^2)	4.27E+05	3.18E+05	6.13E+05
Standard Deviation	8.51E+05	6.27E+05	1.23E+06
Mean Masked Area (m^2)	2.02E+08	1.67E+08	1.90E+08
Standard Deviation	1.86E+08	1.68E+08	1.74E+08
Maximum NDVI >0.2 Area (m^2)	4.34E+06	3.38E+06	7.64E+06

1.2 Landsat ETM to OLI calibration and adjustment for time-series consistency

To ensure consistency across the timeseries, Landsat TM and ETM Tier 2 Top of Atmosphere (TOA) imagery was radiometrically calibrated to OLI imagery using previously published calibration coefficients[2]. This calibration was then evaluated for regions where images from Landsat 7 and Landsat 8 satellites overlapped. No suitable overlapping images were found covering the AP study region, therefore, three alternative sites were chosen. These sites represent: the closest region geographically (southern Chile and Argentina) including the Ushuaia biogeographical region which has abundant *Sphagnum* bogs[3], the sub-Antarctic Kerguelen Islands where similarly low-stature bryophytic vegetation is prevalent[4], and a site in the Canadian Arctic with moss, lichen and graminoid dominated vegetation akin to what has been observed in the Antarctic Peninsula[5,6]. Suitable overlapping Tier 2 TOA imagery was only available for the southern Chile and Argentina scene. Hence, to generate enough results for reliable comparison, Tier 1 TOA imagery was compared for the other two locations. From the above, a further calibration for Landsat 7 derived vegetated area measurements was established using the difference between the peak NDVI value for the overlapping images

(Supplementary Figure 1.1). This value was used to determine the shift required to match the distributions and the percentage of pixels that would additionally pass the NDVI > 0.2 threshold.

Supplementary Figure 1.1 compares the distribution of NDVI values for calibrated Landsat 7 and Landsat 8 scenes in the aforementioned areas. Even when the radiometric calibration[2] was applied, the measured cumulative area of pixels above the 0.2 threshold used by this study was approximately ten percent lower for Landsat 7 than Landsat 8 (Supplementary Table 1.2). Hence, area values from 1986 to 2013 were increased accordingly.

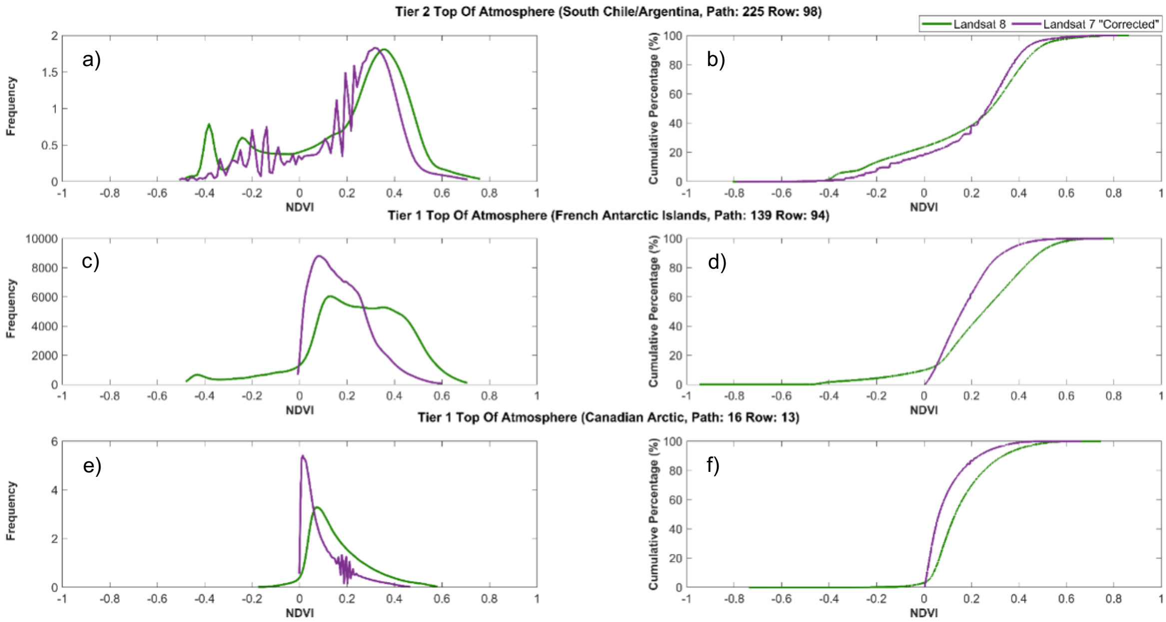

Supplementary Figure 1.1. NDVI value distributions for overlapping Landsat 7 and Landsat 8 scenes. Panels a), c) and e) illustrate the frequency of NDVI values for calibrated Landsat 7 (purple lines) and Landsat 8 (green lines) scenes. Panels b), d) and f) show the cumulative percentage of pixel NDVI values for calibrated Landsat 7 (purple lines) and Landsat 8 (green lines) scenes.

Supplementary Table 1.2. Percentage difference in measured vegetated area for overlapping Landsat 7 and 8 scenes shown in Supplementary Figure 1.1. *Potential additional error with bimodal distribution of NDVI values for the Kerguelen Islands scene.

Image (path, row)	Peak Shift	Cumulative Percentage Difference (%)
225, 98	0.047	9.90
139, 94	0.047	15.3
(maximum error, 2nd peak)*	0.165*	52.6*
16,13	0.056	3.58
	Mean	9.58 ± 4.77
	(Mean including maximum)*	20.3 ± 19.1*

Additionally, a similar method was conducted for TCG values for the same scenes. TCG distributions matched more closely across the satellite imagery than NDVI (Supplementary Figure 1.2). To establish the difference in TCG area, the difference in percentage of pixels with a TCG greater than zero was calculated (Supplementary Table 1.3). Calibrated Landsat 7 scenes were found to under-measure positive TCG values compared to Landsat 8 by approximately five percent (Supplementary Table 1.3).

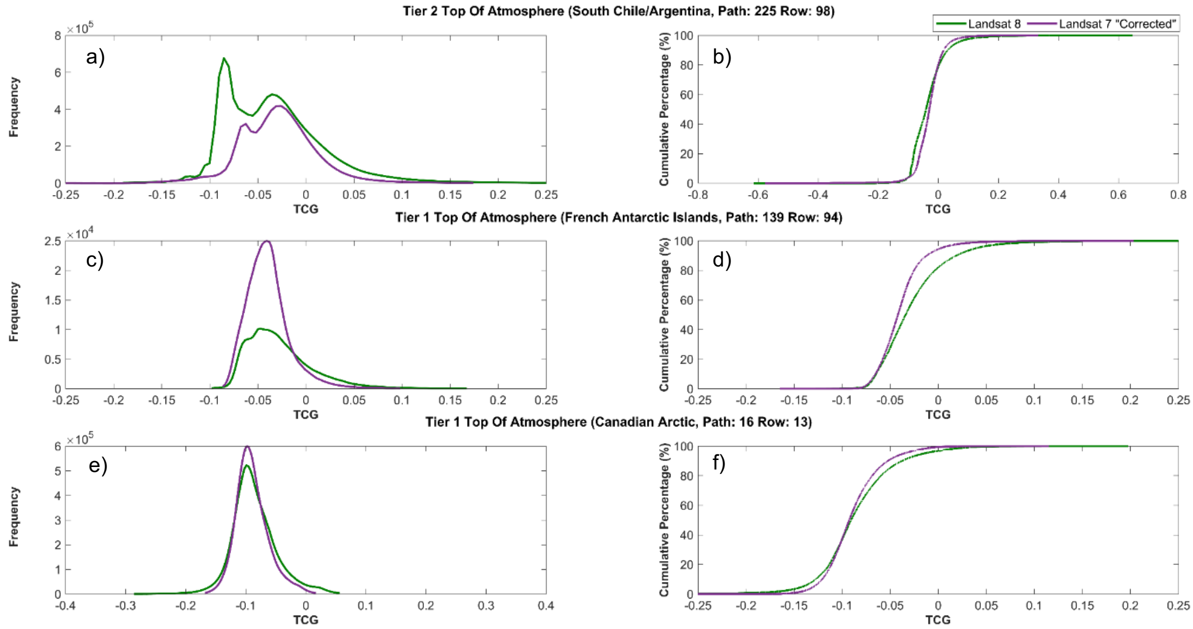

Supplementary Figure 1.2. TCG value distributions for overlapping Landsat 7 and Landsat 8 scenes. Panels a), c) and e) illustrate the frequency of NDVI values for calibrated Landsat 7 (purple lines) and Landsat 8 (green lines) scenes. Panels b), d) and f) show the cumulative percentage of pixel TCG values for calibrated Landsat 7 (purple lines) and Landsat 8 (green lines) scenes.

Supplementary Table 1.3. Percentage difference in measured vegetated area for overlapping Landsat 7 and 8 scenes shown in Supplementary Figure 1.2.

Image	L8 TCG above 0 (%)	L7 (calibrated) TCG above 0 (%)	Difference (%)
225, 98	21.1	19.6	1.58
139, 94	17.9	5.56	12.4
16,13	3.10	0.52	2.58
		Mean	5.68 ± 4.77

Supplement 2. Sampling strategy:

2.1 Methodological approach additional detail

Supplementary Figure 2.1 highlights some of the issues encountered with the data used in this study. Firstly, as the ice-free land polygon[7] is derived using multispectral data, large areas of land can be seen to be missing where there was snow in the images it was mapped from (Supplementary Figure 2.1a). Consequently, large areas of NDVI > 0.2 would not be quantified if this polygon alone was used, illustrated by dark green pixels outside of areas with grey overlay in Supplementary Figure 2.1a. This and the following issues were resolved by generating a 300 m buffer around the ice-free land map (Supplementary Figure 2.1b, c and d). Landsat 4 and 5 Tier 2 TOA imagery covering the region was found to be poorly georectified. Therefore, the 300 m buffer was utilised to capture pixels that would otherwise be miss by the ice-free land map generated from Landsat 8 Tier 2 TOA imagery that is well georectified (Supplementary Figure 2.1b and c). Additionally, this buffer was able to sample all the pixels for an area that appear in erroneous geographic positions due to the scan-line failure on Landsat 7 Tier 2 TOA imagery acquired from 2003-2013 (Supplementary Figure 2.1d). The use of this buffer assumes NDVI values at sea are below 0.2 and/or sufficiently negligible in frequency. Additionally, it assumes the “Fmask” algorithm[8] effectively masks out all snow and ice which falls within the buffer.

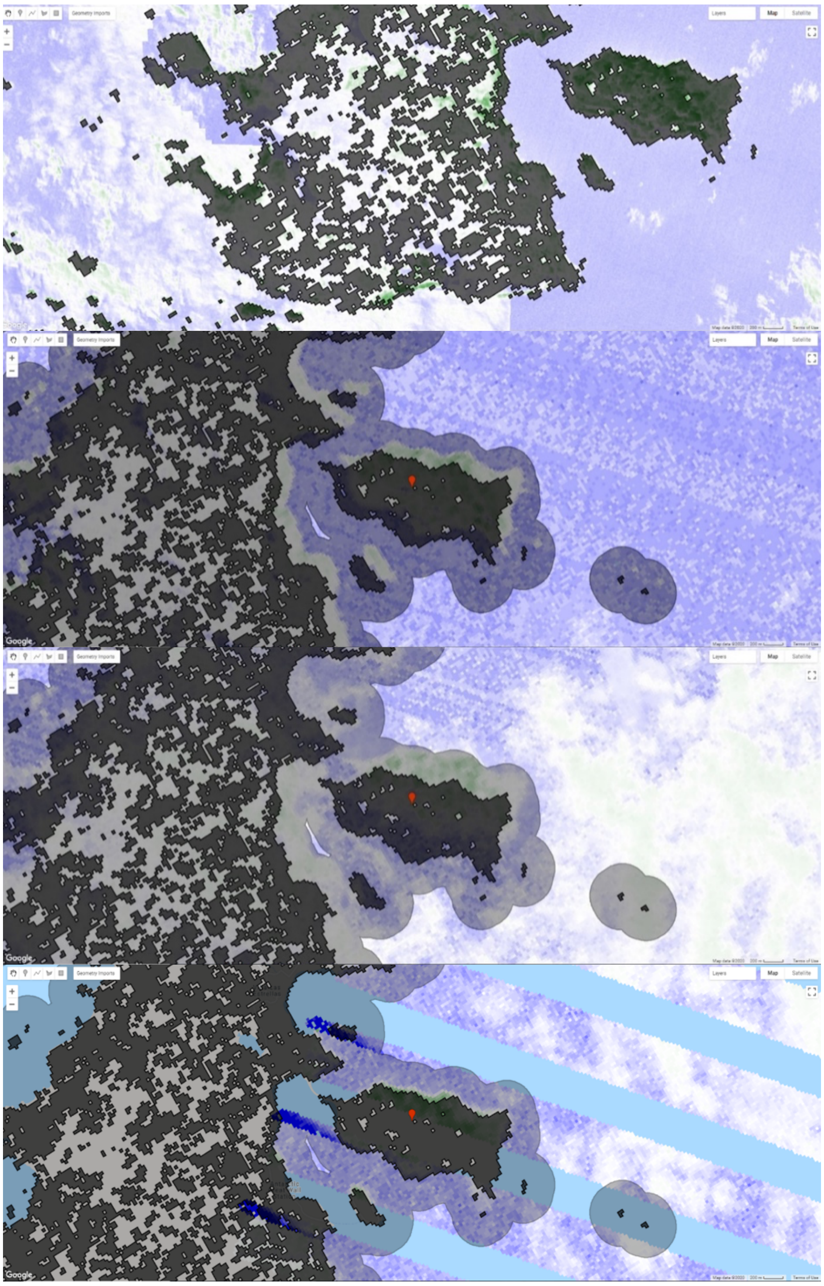

Supplementary Figure 2.1. Examples of errors encountered with Landsat 4,5 and 7 imagery and steps taken to address these. a) Ice-free land map[7] is shown in dark transparent grey over NDVI imagery (blue shading negative NDVI, green shading positive NDVI) for King George Island and Ardley Island. b) The 300 m buffered ice-free land area is shown in light transparent grey over Landsat 4 image derived NDVI. c) Buffered ice-free land and Landsat 5 derived NDVI. d) Buffered ice-free land and Landsat 7 scan-line-correction off image derived NDVI.

2.2 Sampling strategy: elevation mask altitude

At high altitude and latitude bidirectional reflectance errors can generate erroneous NDVI values. Where these values exceed the 0.2 threshold used in this study they would be wrongly counted as vegetation. To limit this effect systematically, the highest altitude of observed moss banks (220 m a.s.l.[9]) was considered along with enough vertical elevation to account for potentially unobserved, higher-altitude vegetation. A 300 m a.s.l. limit was used to account for this. Supplementary Figure 2.2 illustrates the elevation distribution of pixels with NDVI > 0.2 across the annual composites used to generate Figure 3 in the main manuscript. The 300 m limit results in > 99% percent of vegetated pixels remaining detected in 2004, 2016 and 2021. Additionally, this limited the measurement of likely erroneous values at higher altitudes observed in the earlier imagery (1986).

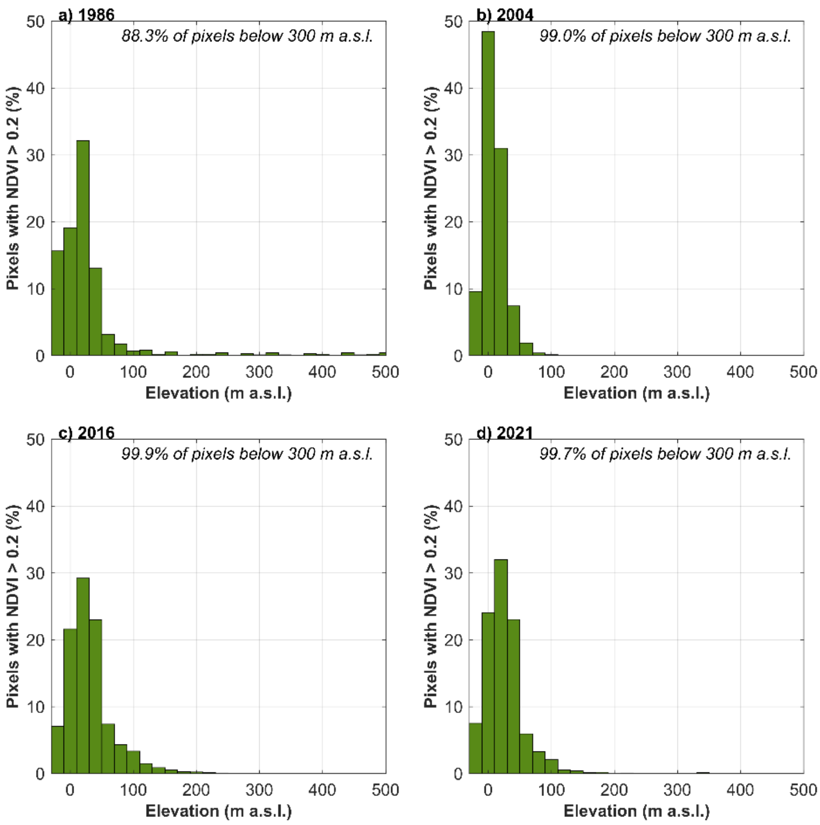

Supplementary Figure 2.2. Elevation distribution of pixels with NDVI > 0.2 across the AP for years mapped in Fig 3. a) 1986, b) 2004, c) 2016, and d) 2021.

2.3 Interannual variation in cloud cover

Persistent cloud cover across the AP[1] presents a considerable challenge to routine monitoring of the land surface in the region using remote-sensing. Supplementary Figure 2.3 illustrates variability in cloud cover through the study period for each sensor, focusing on the month of March (see Supplementary Table 1.1),

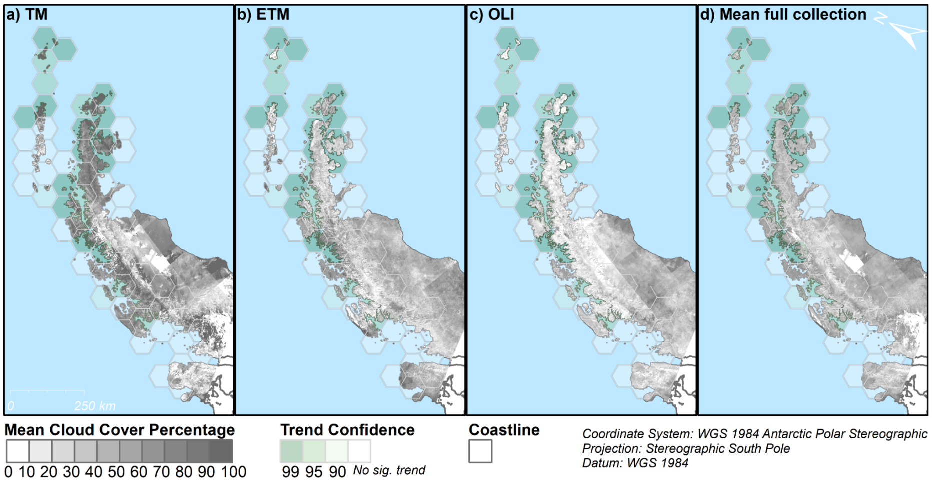

Supplementary Figure 2.3. Mean cloud cover percentage for March images for each sensor, presented against overall greening trend (Fig. 3E in manuscript). a) Landsat 4 and 5 TM, covering years 1986 – 1991 and 1997. b) Landsat 7 ETM+, covering years 2000, 2004 – 2006 and 2009 – 2013. c) Landsat 8 OLI, covering years 2014 – 2018 and 2020 – 2021. d) Mean cloud cover percentage for March in all years of the study.

Supplement 3: Validation

3.1 Landsat 8 and Sentinel 2 comparison

In the absence of field validation, maximum NDVI and TCG composites were generated from Landsat 8 and Sentinel 2 imagery covering 2016 – 2021 for comparison. This was to ensure another instrument would measure similar vegetation extents as the Landsat series utilised by this study. Supplementary Figure 3.1 illustrates a strong positive correlation in NDVI estimated vegetated area (R^2 = 0.758) and a moderate positive correlation for TCG (R^2 = 0.631). However, NDVI area is slightly overestimated by Landsat 8 in comparison to Sentinel 2. TCG areas are typically estimated to be much greater by Sentinel 2 than Landsat 8. Supplementary Table 3.1 highlights the maximum measured areas by Landsat 8 and Sentinel 2 for hexagons where moss banks have been observed in the field. Exact matches were not anticipated, and the outliers are likely the result of a particular hexagon not having sufficiently clear imagery available for a given satellite.

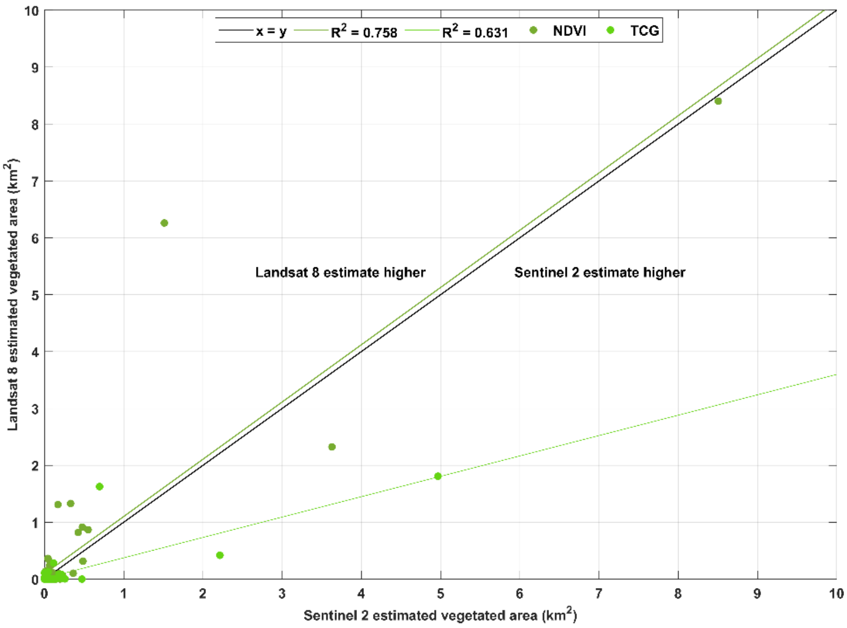

Supplementary Figure 3.1. Correlation of maximum vegetation extents derived using NDVI and TCG indices on Landsat 8 and Sentinel 2 imagery covering 2016-2021.

Supplementary Table 3.1 Landsat 8 and Sentinel 2 maximum area with NDVI >0.2 and TCG >0 from 2016-2021 for hexagons where moss banks have been observed.

Hexagon	NDVI >0.2 Area (km^2)		TCG >0.2 Area (km^2)	
	Landsat 8	*Sentinel 2*	*Landsat 8*	*Sentinel 2*
C3	0.363	0.041	0.029	0.000
C7	8.402	8.504	1.809	4.967
C8	2.323	3.629	0.418	2.214
E12	1.330	0.330	0.127	0.045
F13	0.347	0.049	0.086	0.010
H16	0.014	0.028	0.000	0.006
J19	0.000	0.024	0.000	0.000

3.2 Observed land and total measured area comparison

The total AP land area that crosses our stated greenness thresholds (NDVI > 0.2; TCG > 0) over the study period is partially a function of the distribution of observable ice-free land, which varies from year to year (Fig. 2 in the main manuscript). For example, 2020 appears significantly less green than 2021 (Fig. 2 in the main manuscript) but this is, in part, a result of increased cloud cover over Ardley Island and the Fildes Peninsula – a region with a high proportion of documented moss cover (Fig. 4 in the main manuscript). 2017 has a lower greenness still, with this influential region obscured from view for the entirety of the observation period. To ensure the trend observed in this study was not an artefact of the area of land observed for a given year, observed land percentage was compared with the total area measured by both vegetation indices. A weak positive correlation is observed for NDVI (R^2 = 0.351, p = 0.0029) and no real correlation is observed for TCG (R^2 = 0.272, p = 0.012) (Supplementary Fig. 3.2).

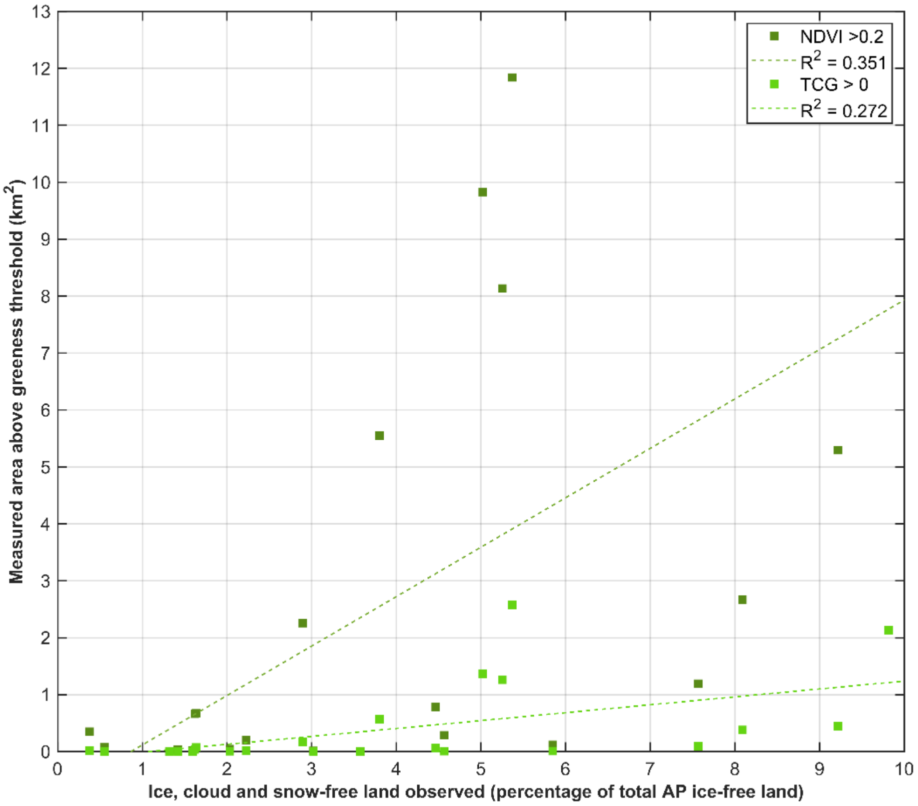

Supplementary Figure 3.2. Correlation of maximum vegetation extents derived using NDVI (dark green) and TCG (light green) indices with the area of ice, cloud and snow-free land observed.

3.3 Very-high resolution supplementary analysis

To further validate the rate and increase of pixels with NDVI >0.2, an independent analysis of very-high resolution imaging data was conducted for an area broadly characteristic of the northern region of the AP, with well-established and observed increases in vegetation in the Landsat archive, and across years spanning the switch from ETM+ to OLI. WorldView-2 images of Robert Island and surrounding islands were acquired for March 2013 and 2016. This analysis mapped NDVI with high precision and a consistent sensor for a transition period in the Landsat series, albeit over a small area.

Supplementary Figures 3.3 and 3.4 show the spectral and spatial response of the two vegetation indices for this area. These highlight the sensitivity of TCG and the significantly reduced extent of vegetation it captures compared to NDVI, supporting our decision to use NDVI as the primary index for our study as well as to keep in line with previous research on vegetation at high latitudes.

In terms of spectral response, TCG only gives a positive value where the red-edge differential is more pronounced, gradient between 655 nm point and 865 nm point (Supplementary Fig. 3.3). Whereas NDVI may still be greater than 0.2 when this differential is reduced. Hence, NDVI is better for capturing a broader scale of "green" pixels, and with a 0.2 threshold is still a conservative estimate. This is reflected spatially in Supplementary Figure 3.4 where areas of NDVI greater than 0.2 are more expansive than areas where TCG is positive. Moreover, most TCG >0 pixels fall within areas where NDVI >0.2. The sensitivity of TCG is particularly noticeable at higher resolutions, highlighting the potential for more extensive coverage of NDVI >0.2 areas than what can be observed at Landsat pixel size (Supplementary Fig. 3.4).

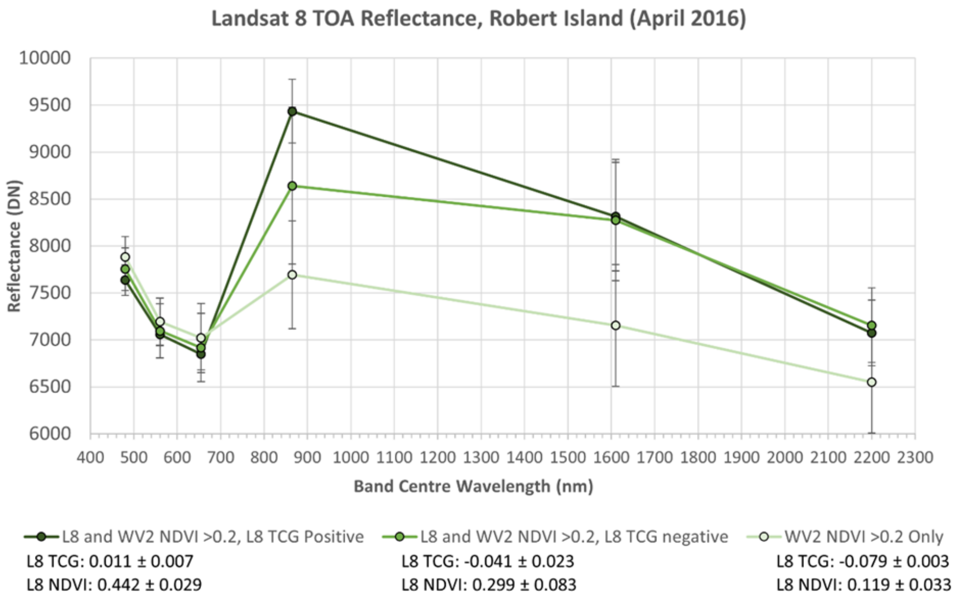

Supplementary Figure 3.3. Mean reflectance values for randomly selected pixels which occur over different vegetation index values. Dark green points, mean of five pixels meeting all vegetation thresholds in the study; medium shade of green, mean of five pixels meeting only the NDVI threshold; lightest green, five pixels where the NDVI threshold is met in WorldView 2 imagery of the location but not in Landsat. Error bars show ± 1σ. Landsat image: LC82191042016077LGN00; WorldView 2 image: 16MAR19130140-P2AS-015353686010.

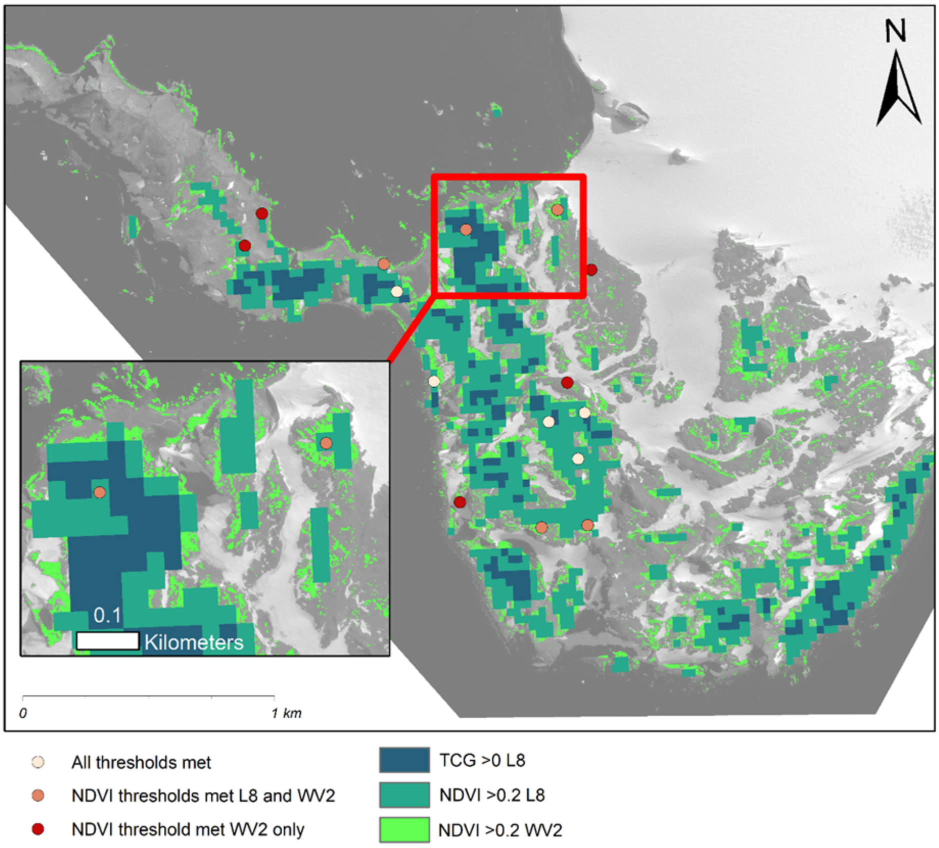

Supplementary Figure 3.4. Vegetation thresholds on Robert Island for Landsat 8 and Worldview 2 imagery, March – April 2016. Landsat 8 pixels which meet the TCG (dark blue) and NDVI (dark teal) thresholds are overlain on the WorldView 2 pixels (light green) which meet the NDVI threshold. Sample points for determining the reflectance averages in Response Fig. 2. are shown in red shades.

For the Robert Island area, from March 2013 and 2016, the area of pixels with NDVI >0.2 increased by 18.7% (0.2 km^2, Supplementary Fig. 3.5). This rate of change is ~8% less than the decadal rate of change measured using Landsat 7 and 8 for the entire AP for the period 2004 – 2016.

Similarly to the spatiotemporal complexity shown in Fig. 4 in the main manuscript, the area of greatest expanse and already well-established vegetation is shown to be relatively stable with slight browning (Supplementary Fig. 3.5). Pixel area with NDVI >0.2 decreased by 0.4% over three years in the southernmost region. However, in regions of relatively new colonization and initially reduced vegetation cover, rapid expansion is observed (regions with smaller pie charts Supplementary Fig. 3.5).

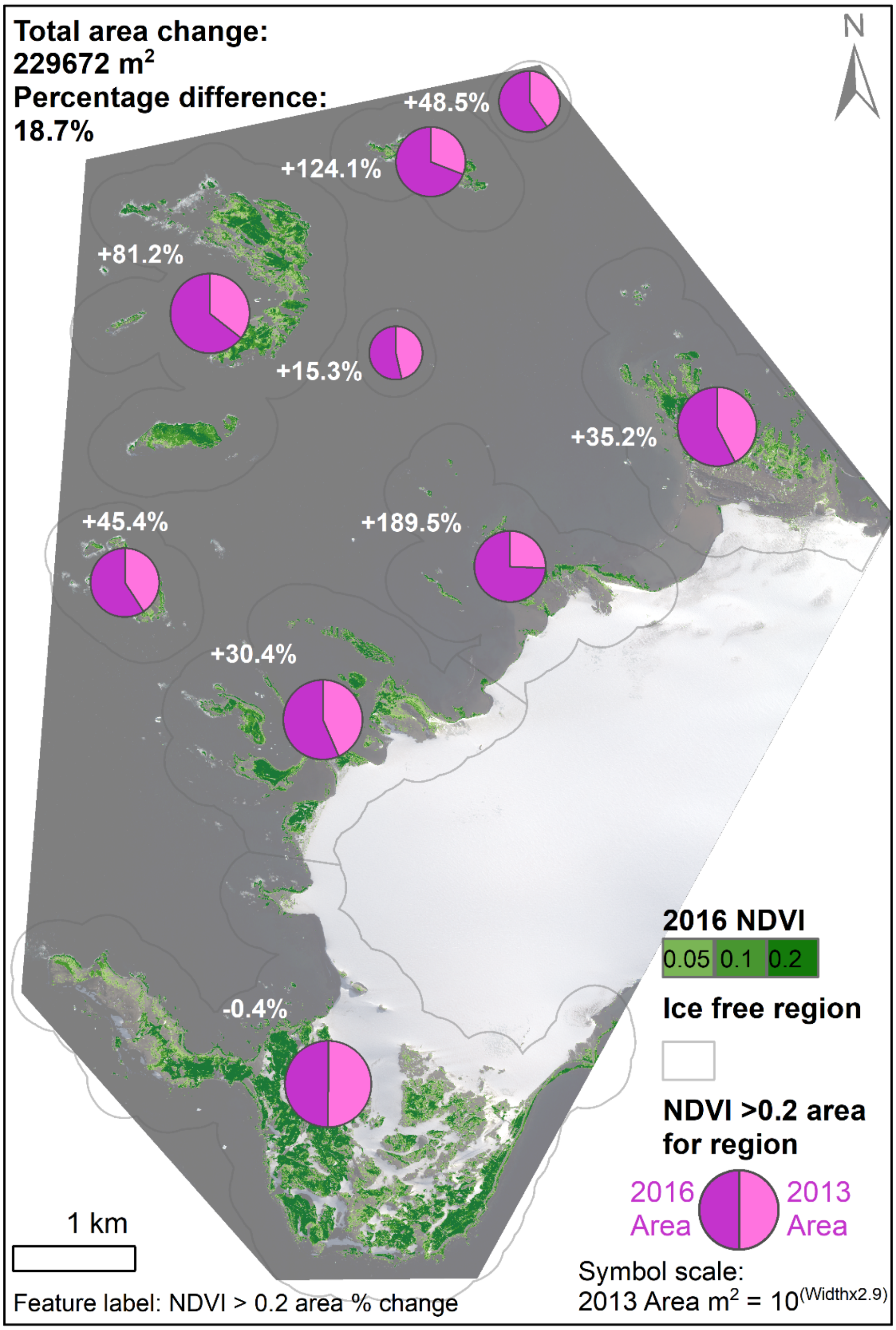

Supplementary Figure 3.5. Areal change in pixels with NDVI >0.2 from March 2013 to March 2016 measured from WorldView-2 images. Green gradation shows the vegetated area in 2016 (darkest green pixels >0.2) and areas of potential vegetation in lighter shades. Pie chart width represents the vegetated area in 2013, with internal scaling comparing the extent in both years. Labels in white indicate the percentage change in area for each region. Regions are arbitrarily divided based on proximity of ice-free areas and isolation of smaller islands.

Supplement 4: Tasselled Cap Greenness (TCG)

Presented here are TCG results discussed throughout the study, which echo and reinforce the NDVI spatial and temporal trends.

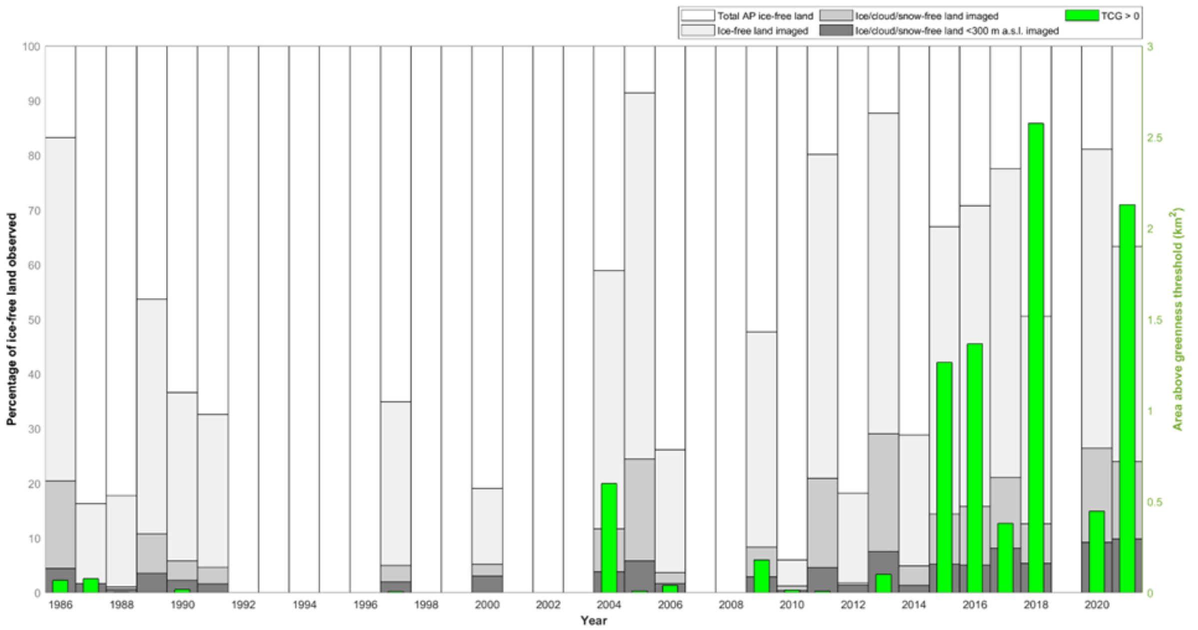

Supplementary Figure 4.1. Change in the areal extent of likely vegetation cover (km^2) based on TCG (>0 threshold, light green bars) across the Antarctic Peninsula derived from Landsat 5-8 data (1986-2021). Grey shaded bars indicate the percentage of ice, cloud and snow-free land observable during March of each year, plotted against total ice-free land on the AP (as measured during austral summer, 2013-2015, using Landsat 8 imagery).

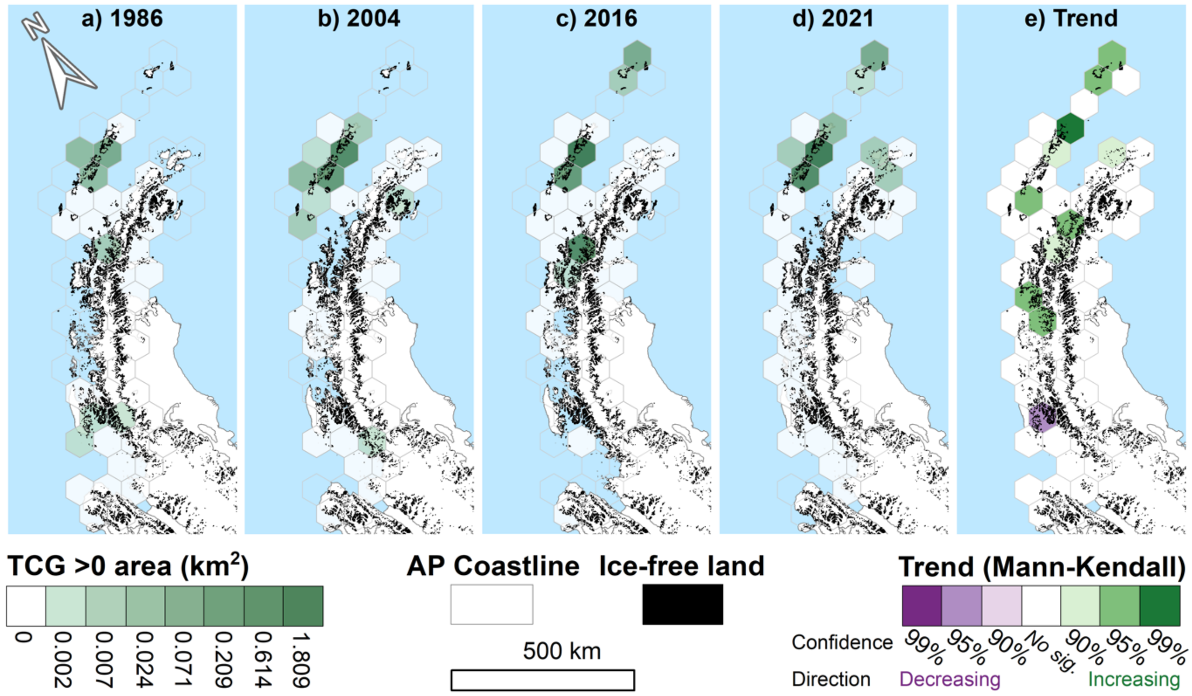

Supplementary Figure 4.2. Spatial and temporal complexity in AP greening trend over the last 35 years. A-D show vegetated area (km^2, <300 m a.s.l.) in the years 1986, 2004, 2016 and 2021 based on Landsat 5-8 data. The hexagons each represent 5000 km2 and are coloured according to the area of TCG >0 they contain, therefore allowing for systematic visualisation of greening trends despite the relatively small proportion of ice-free land compared to ice-covered land and ocean. Years presented follow Figure 3 in the main text. E shows Mann Kendall trend analysis results for all available years (1985 – 2021) showing direction of trend and confidence level.

Supplement 5: Rates of change

Supplementary Table 5.1. Rates of changes in vegetated area across the study region, as calculated from NDVI and TCG. Time periods reflect those highlighted in Figure 3, and the overall study period.

	NDVI > 0.2		TCG > 0	
Time Period	*Area change (km^2 dec^{-1})*	*Percentage change per decade (of maximum extent)*	*Area change (km^2 dec^{-1})*	*Percentage change per decade (of maximum extent)*
1986 - 2021	3.17	26.5	0.589	27.7
1986 – 2004	2.91	24.4	0.298	14.0
2004 – 2016	3.10	26.0	0.634	29.8
2016 – 2021	4.24	35.5	1.53	71.8

Supplementary Table 5.2. Mann-Kendall trend analysis test results for the entire time period and region of study using NDVI and TCG.

Greenness Index	Trend direction	τ	p
NDVI > 0.2 Area	Increasing	2.31	0.021
TCG > 0 Area	Increasing	2.54	0.011

Supplementary Information References

1. Lachlan-Cope, T. Antarctic clouds. *Polar Research* **29**, 150–158 (2010).
2. Roy, D. P. *et al.* Characterization of Landsat-7 to Landsat-8 reflective wavelength and normalized difference vegetation index continuity. *Remote Sens Environ* **185**, 57–70 (2016).
3. Pérez-Haase, A., Iturraspe, R. & Ninot, J. M. Macroclimate and local hydrological regime as drivers of fen vegetation patterns in Tierra del Fuego (Argentina). *Ecohydrology* **12**, 1–17 (2019).
4. Bednarek-Ochyra, H., Plášek, V. & Guo, S. L. A brief survey of bryological studies in the Subantarctic, including Macrocoma tenue (Orthotrichaceae), a moss genus and species newly found in Îles Kerguelen. *Acta Societatis Botanicorum Poloniae* **87**, 1–17 (2018).
5. Broll, G., Tarnocai, C. & Mueller, G. Interactions between vegetation, nutrients and moisture in soils in the Pangnirtung Pass Area, Baffin Island, Canada. *Permafrost and Periglacial Processes* **10**, 265–277 (1999).
6. Liu, N. & Treitz, P. Remote sensing of Arctic percent vegetation cover and fAPAR on Baffin Island, Nunavut, Canada. *International Journal of Applied Earth Observation and Geoinformation* **71**, 159–169 (2018).
7. Burton-Johnson, A., Black, M., Peter, T. F. & Kaluza-Gilbert, J. An automated methodology for differentiating rock from snow, clouds and sea in Antarctica from Landsat 8 imagery: A new rock outcrop map and area estimation for the entire Antarctic continent. *Cryosphere* **10**, 1665–1677 (2016).
8. Zhu, Z., Wang, S. & Woodcock, C. E. Improvement and expansion of the Fmask algorithm: Cloud, cloud shadow, and snow detection for Landsats 4-7, 8, and Sentinel 2 images. *Remote Sens Environ* **159**, 269–277 (2015).
9. Amesbury, M. J. *et al.* Widespread Biological Response to Rapid Warming on the Antarctic Peninsula. *Current Biology* **27**, 1616–1622 (2017).